J. Phys. B: At. Mol. Opt. Phys. **43** (2010) 115003 (11pp) doi:10.1088/0953-4075/43/11/115003

Multiphoton population transfer in a kicked Rydberg atom: adiabatic rapid passage by separatrix crossing

Türker Topçu and Francis Robicheaux

Department of Physics, Auburn University, AL 36849-5311, USA

E-mail: turker@physics.auburn.edu

Received 5 February 2010, in final form 7 April 2010
Published 19 May 2010
Online at stacks.iop.org/JPhysB/43/115003

Abstract

Following an experimental observation, a recent simulation has shown that efficient population transfer can be achieved through adiabatic chirping of a microwave pulse through a 10-photon resonance connecting two Rydberg states with $n = 72$, $\ell = 1$ and $n \sim 82$. These simulations have revealed that this population transfer is essentially a classical transition caused by separatrix crossing in the classical phase space. Here, we present the results of our fully three-dimensional quantum and classical simulations of coherent multiphoton population transfer in *a kicked* Li atom in a Rydberg state. We were able to achieve ∼76% population transfer from the 40p to 46p state in Li through a 6-photon resonance and contrast our results with those when the transition is driven by microwaves. We further discuss the case when the atom starts out from a Stark state in conjunction with the ℓ-distribution of the transferred population. We use a one-dimensional classical model to investigate the classical processes taking place in the phase space and find that the same separatrix crossing mechanism observed in microwave transitions is also responsible for the transition when the atom is kicked.

1. Introduction

Interest in the kicked Rydberg atoms, i.e. the highly excited atoms subjected to electric field pulses much shorter than the Rydberg period of the electron, has been two-fold. From the basic physics standpoint, the interest stems from the fact that Rydberg atoms provide perfect test subjects for studying quantum–classical correspondence. Such studies are especially fruitful when the classical dynamics of the system exhibits crossover between different dynamical regimes, for instance from regular to chaotic dynamics. One of the well established outcomes of these investigations is the observation that the survival probability of a unidirectionally kicked Rydberg atom exhibits a broad maximum with increasing number of kicks when the kick frequency is near the classical orbital frequency of the electron [1, 2]. This is termed dynamical localization and described by a mixed phase space picture where the atom is stable against ionization on one of a series of stable islands. In the long time limit, the atom eventually ionizes due to increased instability in the quantum mechanics which is absent in the classical picture [3]. Very different behaviour is observed when the atom is kicked bidirectionally [4]. In this case, the population gets localized near continuum prior to ionization [5] and no distinct signature of localization is observed. Theoretical calculations supporting experimental observations mostly utilize quasi-one-dimensional models [2, 6] although three-dimensional quantum calculations also exist which are in agreement with these models [7].

From the application standpoint, Rydberg wave packets can be used in the realization of non-dispersing atomic wave packets. These wave packets show promise in applications such as information storage in cavities, as well as precision spectroscopy [8, 9]. In recent experiments, Dunning *et al* achieved a very remarkable level of control in creating very high-n Rydberg wave packets ($n > 300$) by exposing atoms to a series of kicks (see [10] and references therein). They showed that by manipulating the mixed phase space, they could change the period of the wave packet by transferring it between different islands of stability in phase space [11]. They can also focus a wave packet by first loading it onto a stable island and drag it to a desired region of phase space, and changing the size of the island they can focus the wave packet [12]. Their experiments have also been successful in creating

long-lived Bohr-like circular orbits. To this end, they first excite potassium atoms to lowest lying states in the $n = 306$ Stark manifold in the presence of a weak dc field [13]. By suddenly turning on a much stronger dc field in the z-direction, they mix these states into a non-stationary mixture of Stark states which beats between highly elliptical and circular superpositions in time scales of the Stark precession period. Turning off the dc field at roughly half the Stark precession period leaves the atom in near-circular orbits with a maximum value of L_z. They observe the wave packet through the oscillations of $\langle x(t)\rangle$ and $\langle z(t)\rangle$ for several periods before its dephasing due to non-equispaced nature of the energy levels. They support their results with classical simulations.

In this paper, we aim to achieve population transfer between Rydberg states using electric field kicks which we chirp through a multiphoton resonance. Such population transfer in microwave-driven Li Rydberg atoms via multiphoton adiabatic rapid passage has recently been experimentally realized by Maeda *et al* [14]. In this process, only a single multiphoton transition is required to coherently transfer population, as opposed to many concurrent single-photon transitions by chirping the driving field through a number of resonances. The advantages of driving the population through a single-multiphoton resonance as opposed to through a ladder climbing scheme include a substantially reduced chirp range and reduced sensitivity to small changes in the field strength and coupling in experiments. A recent calculation [15] has shown evidence supporting the observations of Maeda *et al* and the claim that this is caused by an adiabatic passage through a multiphoton resonance. These calculations further revealed that starting from a field-free low angular momentum eigenstate of Li atom resulted in a large spread of final angular momenta, which was explained in terms of virtual transitions between the ac Stark-shifted levels. The authors also studied the one-dimensional classical phase space for this system and found that the physics behind the population transfer can be explained classically in terms of the crossing of the separatrix between the islands of stability formed at an energy between those of the initial and the final states. The narrow band of populated final states following the classical transition entirely relies on swinging around this island of stability. Although the island undergoes a small shift in action due to driving, chirping the microwaves by a small amount corrects this and strongly enhances the efficiency of the transfer. For example, ramping the microwave pulse up and then down will only give ∼50% transfer on average unless timing and strength of the pulse is accurately tuned. On the other hand, introducing a small chirp in a microwave pulse can result in almost complete population transfer without the need for fine control.

We demonstrate that this same process can also be made to work when the atom is kicked instead of being driven by microwaves. In the next section, we present results from our three-dimensional quantum calculations. We start from the $n = 72$, $\ell = 1$ state in Li and drive the population up to $n = 80$ by adiabatically chirping the microwave field through an 8-photon resonance condition. Then we decrease the duration of the half-cycles of the microwave to get closer to the impulsive regime while keeping the pulses bidirectional. We try to excite the $n = 40, \ell = 1$ state up to $n = 46$ through a 6-photon resonance condition using unidirectional electric field kicks and discuss that a relatively larger jump in energy prevents efficient transfer. We also try to increase the efficiency by starting from Stark states instead of the field-free eigenstates of Li but do not observe improvement in the transfer efficiency over the case when the initial state is an eigenstate. We achieve ∼76% transfer from the $n = 40, \ell = 1$ state to the $n = 46$ manifold with little spread in ℓ when we decrease the number of kicks and the rate by which we chirp the kicks relative to the microwave-driven case. Then in section 3, we present three-dimensional classical trajectory Monte Carlo (CTMC) simulations for the 8-photon transition from $n = 72$ to $n = 80$. We gradually change microwave pulses to narrower $\cos^3(\omega t)$ impulses and observe the same suppression of excitation as in quantum calculations. We find large differences in the amount of transferred population and final state distributions from the microwave-driven case, which makes this investigation interesting.

Finally in section 4, we investigate the one-dimensional classical model for both the 8-photon transition in section 3 and the 6-photon $n = 40$ to $n = 46$ and 4-photon $n = 40$ to $n = 46$ transitions. We observe that the same separatrix crossing mechanism is responsible for the classical transition as in the microwave-driven case. We also demonstrate that trajectories stick to the edge of the stable surface breaking into the chaotic sea restricting the population transfer efficiency. Harder kicks help them to mix into the chaotic sea which also destroy most of the stable islands in the phase space resulting in a large spread of final states and ionization.

We use atomic units throughout the paper unless we specify SI units explicitly.

2. Quantum calculation in three dimensions

Three-dimensional quantum calculations were carried out by solving the time-dependent Schrödinger equation as described in [16]. For the sake of completeness, here we briefly recite the theoretical outline. The time-dependent wavefunction can be decomposed in spherical harmonics $Y_{\ell,m}(\theta, \phi)$ as

$$\Psi(\vec{r}, t) = \sum_{\ell} f_{\ell}(r, t) Y_{\ell,m}(\theta, \phi) \tag{1}$$

such that the time dependence is captured in the coefficient $f_\ell(r, t)$. For each angular momentum, $f_\ell(r, t)$ is radially represented on a square-root mesh which puts roughly the same number of mesh points between the nodes of the Rydberg states. A square-root mesh with a radial extent R over N points has a grid spacing of $\delta r = R/N^2$ and the radial coordinate of a point is given by $r_j = j^2 \delta r$. In our simulations, typically δr around $1/300$ au with $R = 10^4$ au and 4×10^4 au for 6- and 8-photon resonance transitions yielded converged results. We have regularly performed convergence checks on the number of angular momenta we needed to include in our calculations as we changed physical parameters such as peak field strength and chirp.

We split the total Hamiltonian into atomic Hamiltonian plus the interaction Hamiltonian whose contributions on the

time evolution of the wavefunction are accounted for through the lowest order split operator technique. In this technique each split piece is propagated using an $\mathcal{O}(\delta t^3)$ implicit scheme. A detailed account of the $\mathcal{O}(\delta t^3)$ implicit method and the split operator technique employed is given in [16].

The interaction Hamiltonian $\mathcal{F}(t)r\cos(\theta)$ couples ℓ to $\ell \pm 1$ with a series of kicks $\mathcal{F}(t)$ which we defined as

$$\mathcal{F}(t) = F_K \exp\left[-\left(\frac{t}{\Delta t}\right)^6\right]\cos^{2\eta+1}(\omega t + \dot{\omega}t^2). \qquad (2)$$

Here F_K is the peak field strength, Δt is $1/2$ of the $1/e$ of the width of the time envelope under which the series of kicks are turned on and off. The central frequency of the transition ω is $\Delta E/N_{\rm phot}$ where ΔE is the energy jump targeted by the transition and $N_{\rm phot}$ is the order of the multiphoton resonance being traversed. We use a linear chirp $\dot{\omega}$ which is s/t_f where the slew range s is approximately 1% of ω and time runs from $-t_f$ to t_f. This choice of time range centres the carrier envelope at $t = 0$, which simplifies the mathematical expression in equation (2). Note that our time envelope has a flat top as opposed to the Gaussian envelope employed in [15] which can result in qualitatively different results. By changing $\eta \in \mathbb{Z}^+$, we can attain microwave driving ($\eta = 0$) or bidirectional impulsive kicks ($\eta \gg 1$). To simulate unidirectional impulsive kicks, we use $\eta = 175$ but only retain the positive part of the kicks. This gives a train of unidirectional kicks with the same frequency as that of the corresponding microwaves-driven case. Using narrower kicks in time requires smaller time steps than in the case of microwaves ($\sim$1/500 of a Rydberg period in [15]). For instance, for impulsive kicks we used a factor of 2 smaller δt than in our microwave calculations, and we have found this to be sufficiently small for attaining converged results.

We evaluate the probability for finding the atom in a state with quantum numbers n and ℓ by projecting the wavefunction onto the field-free eigenstates $\chi_{n,\ell}$ of the atom which are generated on the same radial mesh as $f_\ell(r,t)$ by integrating the time-independent Schrödinger equation. We choose the initial wavefunction to be a field-free eigenstate of Li with principal and angular quantum numbers n and ℓ, and take the model potential bearing the correct quantum defects:

$$V = -\frac{1 + 2\,e^{-\alpha_1 r} + r\alpha_2\, e^{-\alpha_3 r}}{r} - \frac{\alpha}{2r^4}[1 - \exp(-r^3)]^2 \qquad (3)$$

with parameters given in [15]. This gives quantum defects of $\sim$0.40 for $\ell = 0$, $\sim$0.048 for $\ell = 1$ and negligible defects for all other ℓ in Li.

Figure 1 shows the results of two calculations using Li with different types of driving when the initial state $n = 72, \ell = 1$ is driven up to $n = 80$ through the 8-photon resonance condition. All the calculations presented in figure 1 have been performed with $F_K = 2.5$ V cm^{-1} and $\sim$97 ns at the FWHM. The solid line in the upper panel is the time-dependent probability for finding the atom in the initial $n = 72$ manifold when the 8-photon resonance is driven by microwaves ($\eta = 0$ in equation (2)). It is evident from the figure that only $\sim$12% of the entire population is left within the initial $n = 72$ manifold. The dashed curve shows the probability to find the atom in the final $n = 80$ manifold under the same resonance and driving conditions and shows that $\sim$83% of the total population ends up in the $n = 80$ manifold. About $\sim$4% ends up in states adjacent to $n = 80$, i.e. $n = 79$ and $n = 81$. The final distribution of the angular momenta in the $n = 80$ manifold is also depicted in figure 1(b) with stars. As had pointed out in [16] the entire ℓ range allowed has been populated indicating that a lot more than eight photons have been absorbed and emitted during the 8-photon transition.

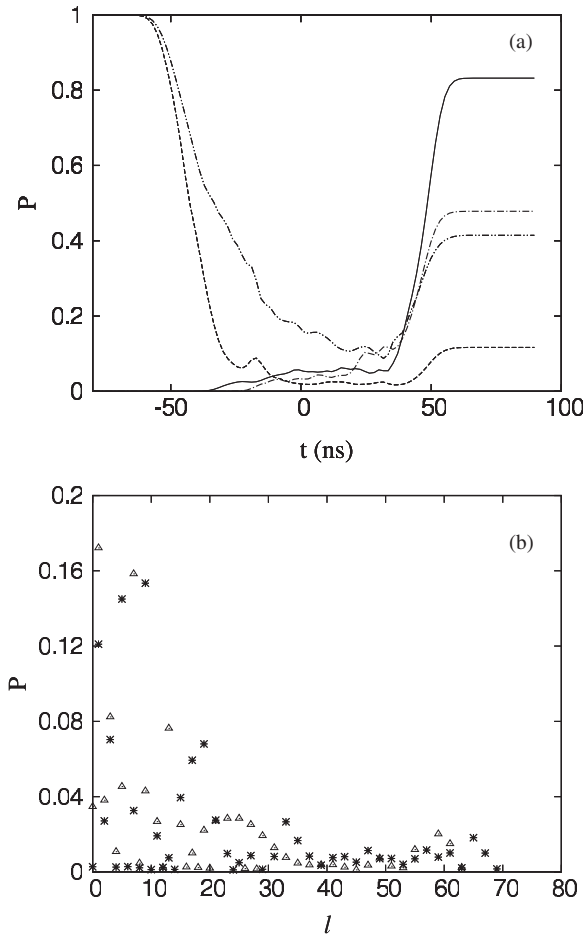

Figure 1. (a) Time-dependent evolution of the probability P for finding the electron in the $n = 72$ and $n = 80$ manifolds of Li for the 8-photon resonance condition. The solid and dashed lines are initial and final n-states when the atom is microwave driven, and dot-dashed and dot-dot-dashed lines when it is subjected to $\cos^3(\omega t + \dot{\omega}t^2)$ pulses. For all these simulations, the peak field strength is 2.5 V cm^{-1} and the time-range runs from -80 ns to 100 ns, during which the carrier envelope peaks at $t = 0$ ns. (b) ℓ-distributions after the driving field is turned off for microwave driven (stars) and $\cos^3(\omega t + \dot{\omega}t^2)$ 'kicked' (triangles) Li. Note that the population has spread out to the entire ℓ-range and only odd-ℓs are substantially populated.

The probability of finding the atom in the $n = 80$ manifold when it is 'kicked' by $\cos^3(\omega t)$ pulses ($\eta = 1$ in equation (2)) is shown with the dot-dashed curves in the upper panel. Every other parameter being the same as in the microwave case, the population transferred into $n = 80$ has dropped to $\sim$45% from $\sim$83%. The corresponding ℓ-distribution is depicted by triangles in the lower panel and mimics the distribution

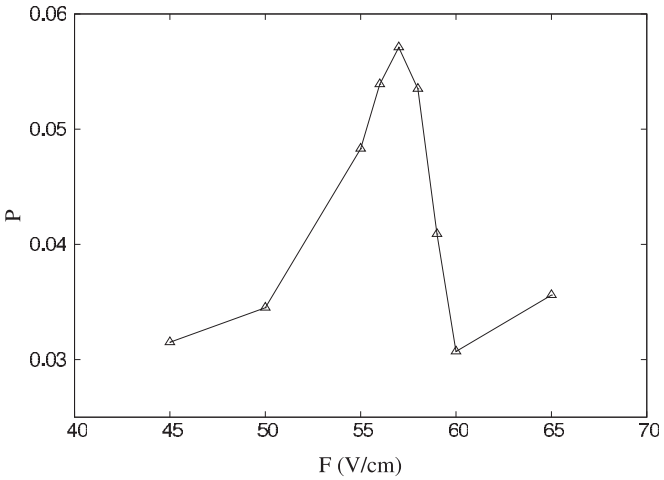

Figure 2. Probabilities to end up in $n = 46$ as a function of the peak field strength F_K for the 6-photon transitioning from 40p to $n = 46$ in Li using unidirectional impulsive kicks.

laid out by the microwave-driven case. In both cases, the ℓ-distributions are confined to odd-ℓ only because the interaction Hamiltonian mixes each ℓ with $\ell \pm 1$ and the initial state is a p-state.

We also considered a case where the ΔE jump caused by the transition is larger than that in figure 1. In particular, we considered transitioning from $n = 40, \ell = 1$ to $n = 46$ in Li via a 6-photon resonance condition using unidirectional impulsive kicks ($\eta = 175$ in equation (2) with only positive part of the pulse retained). We found that the probability to end up in $n = 46$ is only a few per cent, and it is maximum for $F_K = 57$ V cm^{-1}. We have observed that for a given set of parameters, the peak field strength F_K, the chirp $\dot{\omega}$ and the envelope width Δt, there is always an optimum set which gives the maximum amount of transfer. For instance, while keeping the chirp and the envelope width constant, we can only increase the peak field strength up to $F_K = 57$ V cm^{-1}, which gives an upper cap of ∼5.7% transfer into $n = 46$. Figure 2 shows the probability to end up in the final $n = 46$ manifold as a function of the peak field strength for this 6-photon transitioning using unidirectional impulsive kicks. The pulse duration is ∼34 ns, and the kicks are chirped from 9.0×10^{-8} au below to 9.0×10^{-8} au above the 6-photon resonance. As mentioned, $F_K = 57$ V cm^{-1} gives the largest probability for transitioning to $n = 46$, and both stronger and weaker peak fields result in smaller population transfer. Contrary to the large angular momentum spreads we have seen in microwave-driven and bidirectional $\cos^3(\omega t)$ 'kicked' cases, the final ℓ-distribution inside the $n = 46$ manifold shows no change in ℓ whatsoever, leaving the population in $n = 46$ entirely in $\ell = 1$. In the impulsively kicked case, we use $\eta = 175$ which gives field impulses a span of ∼0.25% of the Rydberg period of $n = 46$. Using a peak field of $F_K = 57$ V cm^{-1}, the impulse imparted on the electron is $\sim 1.16 \times 10^{-4}$ au whereas the average momentum of the electron in $n = 40$ is $\sim 1/n \sim 2.5 \times 10^{-2}$ au. As a result, by delivering only a half per cent of the average momentum of the electron in $n = 40$, impulsive kicks do not lead to ℓ mixing.

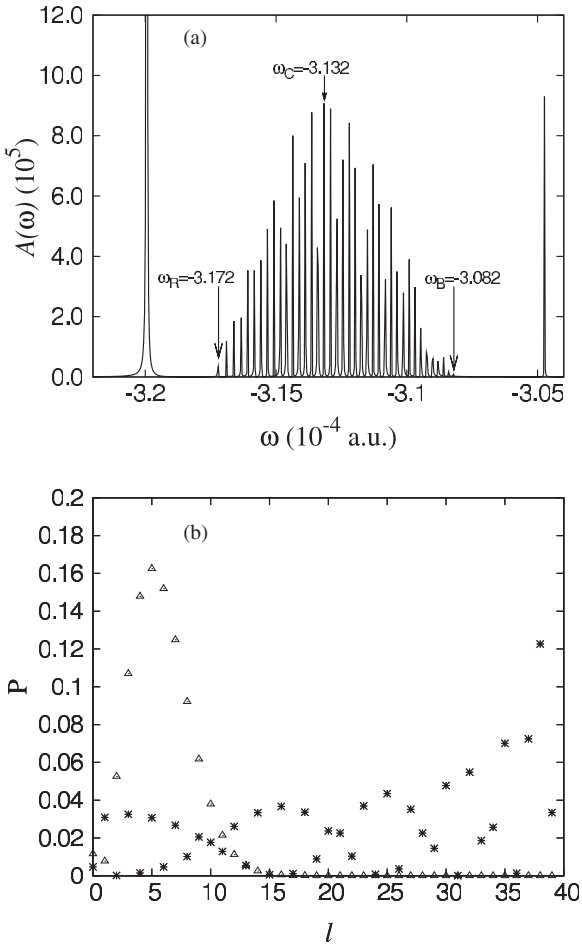

Figure 3. (a) Fourier transform of the autocorrelation function yielding the Stark levels inside the $n = 40$ manifold in a $F_K = 10$ V cm^{-1} static field. The red-most (ω_R), central (ω_C) and blue-most (ω_B) Stark states are pointed out on the spectrum. (b) ℓ-distributions of the red-most (triangles) and central (stars) Stark states. The red-most Stark state is elongated along the polarization axis, whereas the central Stark state has spread out in ℓ with larger emphasis on the high-ℓ end of the manifold.

2.1. Transition from Stark states

Initial states used in figure 1 and in our 6-photon calculations are all field-free eigenstates of Li. The question arises as to whether we can achieve larger transfer into final states if we start from a Stark state.

To generate Stark states, first we start from the $n = 40$, $\ell = 1$ eigenstate of Li and slowly ramp up a dc electric field to mix the initial p-state into other ℓ-states inside the $n = 40$ manifold. The dc field strength we used is 10 V cm^{-1}, and it is too weak to cause n-mixing for $n = 40$. We then evaluate the time-dependent autocorrelation function

$$A(t) = \langle \Psi(\vec{r}, -t_f) \mid \Psi(\vec{r}, t) \rangle. \quad (4)$$

We let the wavefunction beat for several periods of Stark oscillation before we Fourier transform $A(t)$ to obtain the spectral autocorrelation function $\tilde{A}(\omega)$. This gives us the energy spectrum of the Stark levels inside the electric field. Figure 3(a) shows the Stark levels into which the $n = 40$ manifold splits with the red-most (ω_R), central (ω_C), and blue-most (ω_B) Stark levels are marked by arrows. We evaluate the

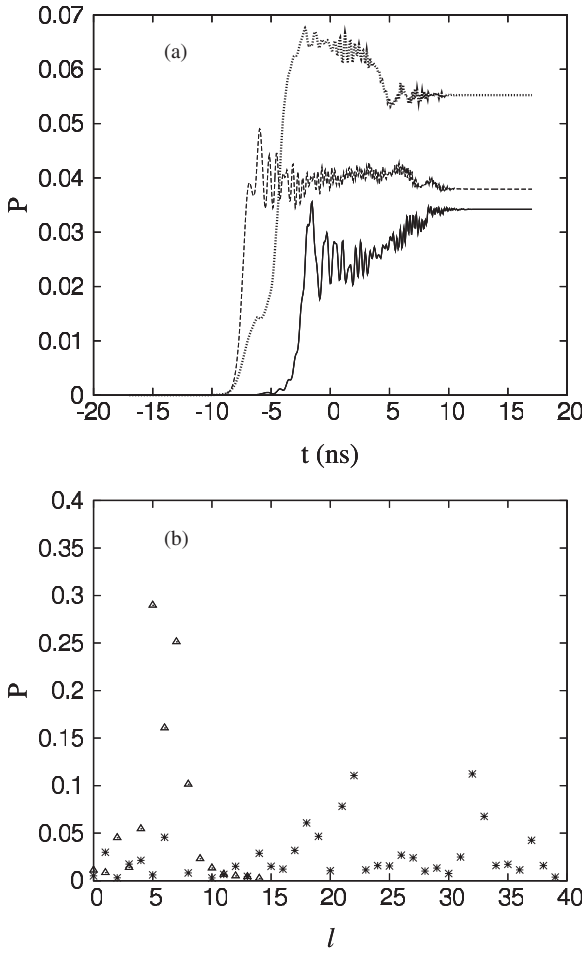

Figure 4. (a) Same as figure 1 but for three different initial states for a peak field strength of $F = 37$ V cm^{-1}. The solid line is when the atom starts from the field-free 40p state, dashed line when it starts from the red-most Stark state and dotted line when it starts from the central Stark state. (b) Final ℓ-distributions when the initial state is the red-most (triangles) and central (stars) Stark states, respectively. As in figure 3 all ℓ are populated irrespective of their parity.

corresponding Stark states by accumulating amplitude into the corresponding Fourier component by evaluating

$$\int_{-t_f}^{t_f} \Psi(\vec{r}, t) \exp[-(t/\Delta t)^2] \exp[i\omega_S t]\, dt \qquad (5)$$

where ω_S is either one of ω_R, ω_C and ω_B. The ℓ-distributions for the red-most (triangles) and central (stars) Stark states are shown in figure 3(b) where we omitted the blue-most Stark states since it too aligns along the same direction as the electric field. Note that the red-most Stark state is made up of small-ℓ compared to the central stark State and is aligned mostly along the direction of the electric field. The dominant angular momenta making up the central Stark state flip between being odd and even about every 10 units of angular momenta.

Figure 4 compares the probabilities of transitioning into $n = 46$ from $n = 40$ through the 6-photon resonance condition for a peak field strength of $F_K = 37$ V cm^{-1} when the Li atom starts from the atomic $n = 40$, $\ell = 1$ eigenstate (solid), red-most (dashed) and the central (dotted) Stark states. In this case, we use a ∼20 ns pulse at the FWHM of unidirectional

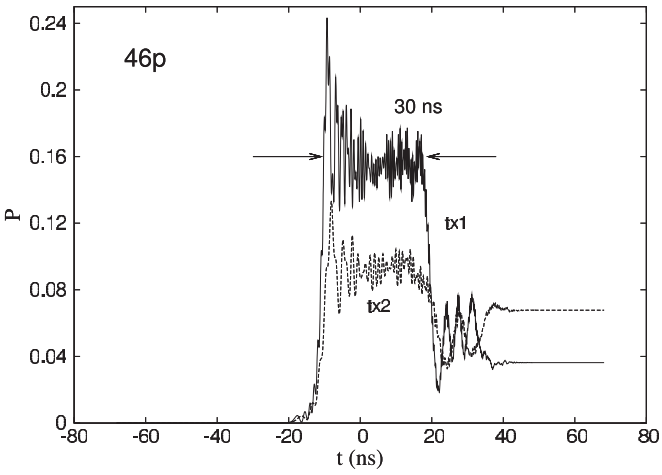

Figure 5. Time-dependent probability for finding the atom in the $n = 46$ state using envelopes with the FWHM of ∼ 68 ns (black curve) and ∼36 ns (dashed curve). The time axis for the dashed curve with shorter envelope has been scaled by 2 in order to contrast with the result obtained using the longer envelope. In both cases, $F_K = 57$ V cm^{-1} and the kicks are chirped through ±1% of the 6-photon resonance connecting $n = 40$ with $n = 46$.

impulsive kicks. Starting from this field-free eigenstate, we achieve about 3.4% transfer, whereas red-most and central Stark states give 3.8% and 5.5% migration of the population respectively. Therefore, initially preparing the atom in a Stark state rather than a field-free eigenstate does not let us transfer larger fraction of the population by impulsively kicking the atom. Also note that the behaviour displayed by the the red-most stark state is most similar to that of the $n = 40$, $\ell = 1$ eigenstate. This would be expected since both have small-ℓ character, i.e. both are mostly aligned along the electric field direction in contrast with the central Stark state. The ℓ-distributions of the final population within the $n = 46$ manifold show that starting from the red-most Stark state composed of low-ℓ states in figure 3(b) maintains the same low-ℓ character, and the large-ℓ distribution of the central Stark state remains largely spread over the final n-manifold. This is in parallel with our previous observation that the angular momentum remains largely unchanged when the atom in a 40p state is impulsively kicked using the 6-photon resonance condition using $F_K = 57$ V cm^{-1}, since figure 4 is for an even more weakly kicked atom.

2.2. An accidental resonance in the long-time limit

Figure 5 shows time-dependent probability for the 6-photon resonance excitation of the 40p state of Li up to $n = 46$ using unidirectional impulsive kicks. The peak field strength is $F = 57$ V cm^{-1}. A solid curve is obtained with an ∼68 ns envelope at the FWHM and a dashed curve using an ∼36 ns envelope. The time axis for the ∼36 ns curve has been scaled by a factor of 2 in order to fit both curves in the same time range. In both cases, the population transferred into $n = 46$ collapses after some time, more prominently for the longer envelope. In the case of ∼68 ns envelope, the population survives for ∼30 ns after the $n = 46$ manifold is populated up

to ∼16%. The probabilities rising at early times do not exactly lie on top of each other due to the fact that the frequency is chirped within ±1% of the 6-photon resonance in both cases. This results in about twice as large slew rate for the shorter envelope compared to the ∼68 ns envelope. The factor of 2 difference in time for the populations to collapse indicates that this effect is a result of different rates of chirping through an accidental resonance. We did not observe this transition in shorter pulses indicating that this transition requires better energy resolution.

When we analyse the n-distribution of the population after the kick pulse is turned off, we see that a significant fraction of the population in the 46p state is excited up to the 52p state. In the case of the ∼68 ns envelope in figure 5, after the pulse is turned off, ∼4% of the population is left in the 46p state, whereas ∼15% ends up in the 52p state. Together with ∼70% of the population staying in the initial 40p state, this adds up to the entire fraction of the population that resides in p-states, which is ∼86%. About 5% of the population ends up in $\ell = 0$ states, and the remaining few per cent distributed among the next few even angular momenta. Also, about 4–5% of the population ends up in the $n = 49$ and $n = 56$ manifolds. The reason behind the sudden transfer of population from the 46p to 52p state is the accidental 4-photon resonance that is swept across during the chirping of the kick frequency. The energy difference between the field-free 46p and 52p states and 4 times the 6-photon resonance frequency differ by ∼0.4%. Since the chirp range is same for both curves in figure 5 and the time axis of the twice as shorter pulse is scaled by a factor of 2, both curves show drop in probability at the same point on the time axis when the accidental 4-photon resonance is swept through.

2.3. Narrow pulse envelope and slower chirp

Another thing to notice in figure 5 is that the largest population transfer is attained right after the kick pulse peaks. Keeping the pulse on after this point by using a flat top envelope as in equation (2) does not result in any net population transfer in or out of the 46p state until the accidental 4-photon resonance is swept through. This prompted us to turn off the kick envelope after it reaches its peak strength. In this way, the population would have no time to transition out of the $n = 46$ manifold, resulting in larger probability to end up in the final state after the pulse is turned off.

To demonstrate this, we use the same case presented in figure 5 with the ∼38 ns pulse envelope. The inset in figure 6 shows the flat-top envelope of equation (2) versus the envelope turned off right after it reaches its peak. The final populations that end up in the 46p state of Li in both cases are plotted with corresponding line styles. The case with the shorter pulse envelope yields ∼16% population transfer, which is approximately a factor of 2 larger than the highest probability achieved before the population collapsed, using the longer flat-top envelope. For the flat-top envelope the frequency is chirped from ∼1% below to ∼1% above the 6-photon resonance frequency. The same rate of chirp was also in order for the shorter envelope. When the envelope was

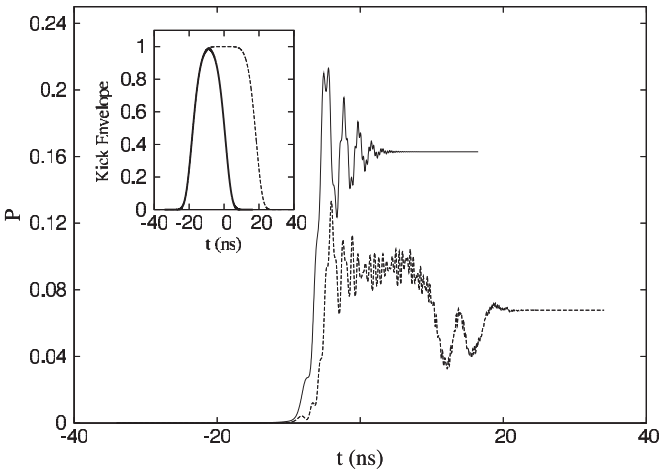

Figure 6. Time-dependent P to find the atom in $n = 46$ for the dashed curve of figure 5. When the envelope is modified such that it falls off right after it peaks (inset), the final P settles to ∼16% compared to ∼7% using the flat-top envelope.

cut short by turning it off after reaching its peak, the frequency has reached only ∼0.4% above the 6-photon resonance at the end of the narrower pulse. The reason for the faster and larger accumulation of population in the case of the narrow envelope is that the probability starts to rise up after the peak of the pulse is reached. Therefore, the improvement comes from the falling edge of the narrow envelope.

Using the same type of narrow envelope as in figure 6 (solid curve) and slowing down the rate at which the kick frequency is chirped, we were able to achieve a large population transfer from the $n = 40, \ell = 1$ state into the $n = 46, \ell = 1$ state of Li. We used an ∼300 ns envelope at the FWHM with $F_K = 70$ V cm^{-1}, and we impulsively kicked the atom with unidirectional pulses. Figure 7 shows the time-dependent probabilities for the atom to be found in the 40p state, $n = 46$ and $n = 50$ manifolds. The initial state 40p has been practically depleted (solid curve) and ∼74% of it ends up in the $n = 46$ manifold with $\ell < 5$ (dashed curve). Note that the transition takes place over a rather short period of time near ∼100 ns after the pulse envelope peaks. The distribution of population in n and ℓ are shown in insets at $t = -104.6$ ns and $t = -92$ ns, just before and after the transition. About ∼12% of the total population ends up in the $n = 50$ manifold. This comes from an accidental 4-photon resonance: the 6-photon resonance frequency is 1/4 times the transition frequency from $n = 46$ to $n = 50$ to within ∼5%. This transition is possible because of the $\cos(3\omega t)$ component in the impulsive kicks. Through the trigonometric identity $\cos^3(\omega t) = (3/4)\cos(\omega t) + (1/4)\cos(3\omega t)$ and the fact that our impulsive kicks can be written as an integer power of $\cos^3(\omega t)$, the kicking pulse bears this $\cos(3\omega t)$ component. Since the $\cos(3\omega t)$ component cannot take a p-state into another p-state, the transition into $n = 50$ results in population with a large ℓ spread (see the inset at $t = 173.6$ ns).

One concern raised by Dunning *et al* [10] regarding experiments to study impulsively kicked Rydberg atoms with moderate n ($n \sim 30$) is that electric field pulses which can be

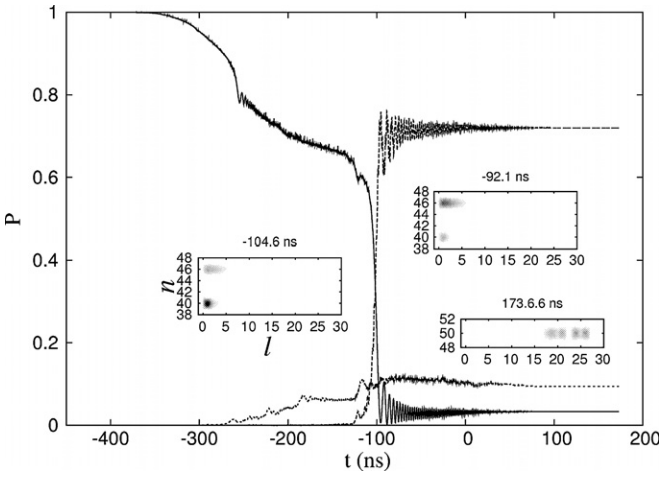

Figure 7. Similar to the solid curve in figure 6 but using an envelope with the FWHM of ∼300 ns and $F_K = 70$ V cm^{-1}. The initial 40p state is almost completely depleted (solid curve) and ∼74% of the population ends up in the $n = 46$ manifold with $\ell < 5$ (dashed curve). The n, ℓ-distributions just before and after the transition takes place are seen in the insets. Probability to end up in $n = 50$ is also shown (dotted curve) with its final large ℓ-distribution.

considered impulses for this n regime can only be generated as unipolar pulses which are followed by a weaker and much longer pulse of opposite polarity. They argue that this weaker long half-cycle pulse (HCP) can complicate the level dynamics involved. In the case of figure 7, the Rydberg period for $n = 40$ is ∼9.7 ps and the energy separation between adjacent n-manifolds is roughly $1/n^3 \sim 1.6 \times 10^{-5}$ au. Therefore, in order for n-mixing to occur, one needs to apply a dc field of at least ∼17 V cm^{-1}. We kick the 40p state of Li with an impulsive kick of $F_K = 70$ V cm^{-1}. Typical amplitude asymmetry between the short and long half-cycles in unipolar pulses is roughly 13:1 [17]. This means the the long half-cycle of the kick would have a typical amplitude of ∼5.4 V cm^{-1}, which is well below the n-mixing regime for the $n = 40$ manifold. The energy separation $\Delta E_{r,b}$ between the red-most and the blue-most Stark states inside the $n = 40$ manifold in this field is $\sim 3Fn(n-1) \sim 4.8 \times 10^{-6}$ au and this is less than the energy spacing between the adjacent n-manifolds. Hence, we can conclude that kicking the 40p state with a realistic unipolar impulse of $F_K = 70$ V cm^{-1} as in figure 7 will not give rise to n-mixing that is not a result of the shorter trailing half-cycle. On the other hand, the typical duration ratio between the short and long half-cycles in realistic unipolar pulses is however 1:140 [17]. Given that our kicks take up ∼4% of the Rydberg period, the long half-cycle would last about 54 ps. This is about 1/23 of the Stark beating period $2\pi/(3Fn) \sim 1220$ ps in $n = 40$ when $F_{\rm dc} = 5.4$ V cm^{-1}. As a result, ℓ-mixing will be induced by the long half-cycle, but only in such a way that starting from $\ell = 1$, the mixing is not likely to exceed $\ell \sim 5$.

3. Classical calculations in three dimensions

We also investigate classical probability distribution in effective n for the 8-photon resonance transitioning from

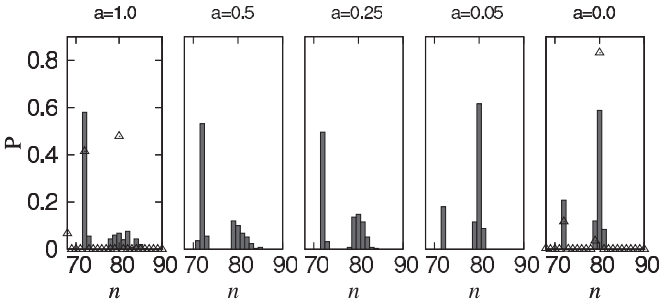

Figure 8. Probability as a function of effective n from 3D CTMC calculations for 8-photon resonance transitioning from $n = 72$ to $n = 80$ for various values of a ranging from 1 to 0. The peak field strength is 2.5 V cm^{-1} as in figure 1 for all cases. The progression from $\cos^3(\omega t + \dot{\omega} t^2)$ ($a = 1$) to $\cos(\omega t + \dot{\omega} t^2)$ ($a = 0$) displays vindication of the efficient population transfer into $n = 80$ as the microwave driving of the atom is achieved. Panels for $a = 1$ and $a = 0$ also show the n-distributions from the full three-dimensional quantum simulations of figure 1.

$n = 72$ to $n = 80$. We use a driving field of the form

$$\mathcal{F}(t) = F_K \exp\left[-\left(\frac{t}{\Delta t}\right)^6\right] \times \left[\frac{a}{4}\cos\{3(\omega t + \dot{\omega} t^2)\} + \frac{4-a}{4}\cos(\omega t + \dot{\omega} t^2)\right]$$

where we vary a from 1 to 0. When $a = 1$, this gives bidirectional $\cos^3(\omega t + \dot{\omega} t^2)$ pulses, and when $a = 0$, it reverts back to microwave driving. Results of three-dimensional CTMC simulations including three more intermediate values of a are shown in figure 8 where we use a flat-top pulse envelope of ∼36 ns at the FWHM and $F_K = 2.5$ V cm^{-1}. For $\cos^3(\omega t + \dot{\omega} t^2)$ pulses ($a = 1$), only about 5% transfer into $n = 80$ is achieved with a total of 40% of the population spreading over the $n = 79$–85 band. Larger and larger fraction of the population is transferred into $n = 80$ with narrower spread in final n as a is decreased. When $a = 0$, the bidirectional pulses become microwaves, which result in almost ∼60% transfer into the $n = 80$ state. Final n-distributions from the quantum simulations are shown as triangles for the corresponding $a = 1$ and $a = 0$ cases in figure 8. For the microwave-driven case with $a = 0$, neither classical nor quantum distributions show a substantial n spread with a high efficiency of population transfer. In the $a = 1$ case, the quantum results do not display a large spread in n compared to those from the classical simulations. Almost the entire population stays in states with $n = 72$ and 80 with a smaller fraction transitioning into $n = 80$ compared to the microwave-driven case. Classical population transfers with similar efficiencies for microwaves were previously reported in 3D classical simulations [15].

Driving $n = 40$ to $n = 46$ via the 6-photon resonance condition using microwaves, we observe no transition out of $n = 40$ until we reach $F_K = 42$ V cm^{-1}. When we start to exceed this threshold of microwave driving strength, significant fractions of the population start to ionize and a wide band of states with $n > 44$ is excited. Roughly 20% of the trajectories ionize and ∼40% are exited to states with $n > 44$.

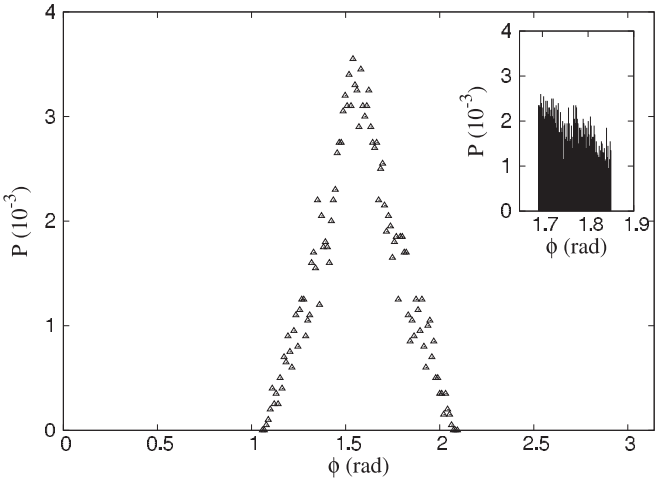

Figure 9. Angular distribution of the launched trajectories which transition to $n > 76$ using kicks with $F_K = 2.5$ V cm^{-1} under the 8-photon resonance condition discussed in the text. Probability peaks around $\pi/2$ as would be expected and shows the irregular structure as displayed by the inset for a smaller angular range.

Angular distribution of the trajectories which end up with $n > 76$ when $a = 1$ in figure 8 is seen in figure 9. The angle ϕ is the angle which the r-coordinate of the trajectory makes with the z-axis when it is launched. For example, when $\phi = \pi/2$, the trajectory is launched along the direction of the bidirectional $\cos^3(\omega t + \dot{\omega} t^2)$ pulses. All the trajectories are launched perpendicular to the x-axis from within the xz-plane. There are 200 trajectories for 100 angular bins, each spanning a range of $\delta\phi \sim 10^{-2}$ rad. When a trajectory starts from a point along the pulse axis, the ionization probability is maximum as expected. As the angle ϕ deviates from $\pi/2$ by $\pm\pi/3$, the probability to end up with an energy corresponding to $n > 76$ drops quickly and becomes zero when ϕ becomes $\pi/6$ or $5\pi/6$. The inset in figure 9 zooms into a smaller ϕ range around $\phi \sim 1.7$ with narrower angular bins to resolve any underlying structure in the distribution. There are 100 angular bins in the inset spanning $\delta\phi = 1.6 \times 10^{-3}$ rad each. They have 200 trajectories in each with launch times randomized over one Rydberg period of the initial $n = 72$ state. Note that there are two narrow ranges of ϕ on both the rising and falling edges of the distribution which display noticeably larger statistical fluctuations compared to the rest of the distribution. This points out to a structure in the angular distribution. We speculate this to be similar to those observed in the numerical simulations of ionization from a hydrogen atom in parallel electric and magnetic fields. In [18], Mitchell *et al* observed self-similar fractal structures in the time it takes for an escaping trajectory to hit the detector as a function of the launch angle. Their system is an example of an open system which is known to display classical chaos, whereas our problem is an example of a closed system with a mixed phase space structure.

4. Classical calculations in one dimension

The classical mechanism behind the population transfer using microwaves has been explained in [15] using a one-dimensional classical model and tracing the trajectories in phase space. In this model, the authors used action-angle variables as the conjugate coordinates to plot surfaces of sections. Field-dependent action-angle variables are derived in [19] for a hydrogen atom interacting with microwaves and are given by $I = 1/\sqrt{-2E}$, $\theta = 2\pi - 2[\sin^{-1}(\sqrt{\beta}) - \sqrt{\beta(1-\beta)}]$ for $v < 0$ and $\theta = 2[\sin^{-1}(\sqrt{\beta}) - \sqrt{\beta(1-\beta)}]$ for $v > 0$. Here, v is the velocity of the electron and $\beta = -xE$. Note that I is the effective quantum number n. In our simulations, we use hydrogen as described in [15] and do not chirp either the microwaves or the kicks.

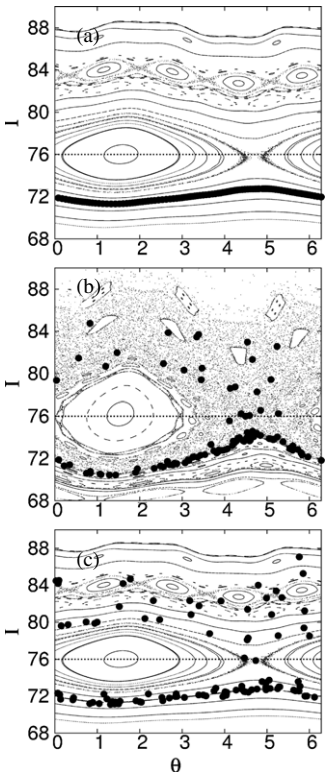

Figure 10. Phase space positions of the trajectories from the 1D classical model at the rising edge (upper panel), peak (middle panel) and falling edge (bottom panel) of the envelope for the 8-photon transitioning with $F_K = 1.1$, 2.5 and 1.1 V cm^{-1} respectively. The large points overlayed on top of the Poincarè surfaces of section are actual trajectories at these instances during the pulse. The dotted line marks $I = 76$ and the centre of the island does not move very much. Note that a large fraction of the trajectories linger at the border where $I = 72$ mixes into the chaotic sea.

In figure 10, we plot phase space positions of an ensemble of trajectories which start with $I = 72$ and are 'kicked' with bidirectional $\cos^3(\omega t)$ pulses with $F_K = 2.5$ V cm^{-1} for the 8-photon resonance condition. The positions of these trajectories are plotted on the top of the Poincarè surfaces of section during the rising (top panel), at peak (middle panel) and falling edge (bottom panel) of the pulse envelope. The field strengths at these instances are 1.1, 2.5 and 1.1 V cm^{-1} respectively. As the peak field strength rises, islands of stability are formed before the $I = 72$ KAM surface is destroyed (figure 10(a)). When the peak field strength reaches 2.5 V cm^{-1}, most of the stable structure of

the phase space is destroyed and mixed into the chaotic sea (figure 10(b)). Some of the trajectories that were initially on the $I = 72$ surface mix into the chaotic sea but most of them stay near $I = 72$. The reason for this is that small islands of stability are formed near the interface between the stable and the chaotic manifolds, where the $I = 72$ manifold is mixing into the chaotic sea. This makes the edge of the $I = 72$ surface sticky and results in most of the trajectories getting trapped in this region. As the field strength falls off to 1.1 V cm^{-1} again, most of these trajectories are captured back onto the $I = 72$ surface and a relatively small fraction of the trajectories that made into the chaotic sea are spread over an n-range spanning from $n = 80$ to 84 (figure 10(c)). This behaviour is different than that observed for microwaves in [15] in that here we have a relatively wider spread over the final n, and most of the trajectories stick to the interface between the initial $I = 72$ surface and the chaotic sea. The stickiness of the KAM surface bordering the chaotic sea makes it difficult to mix all the trajectories into the chaotic sea in contrast with the microwave case as depicted in figure 7 in [15]. This is the reason why a large fraction of the trajectories does not transition. Furthermore, due to relatively large peak field strength, most of the stable phase space structure above the main island is destroyed and the chaotic sea extends high up in I. This is the reason as to why we observe a larger spread in final n compared to the microwave case. To drive the multiphoton transition with microwaves, one does not need to drive the system too hard to the point where the stable structures near and above the final n are destroyed. Driving the system too hard results in dissolution of these stable structures into the chaotic sea, letting trajectories drift further up in I. Larger fraction of the trajectories can be mixed into the chaotic sea if the atom is kicked harder, but this further destroys the stable island structures in the phase space resulting in the larger spread in final n and eventually gives rise to ionization.

For the 6-photon transitioning from $I = 40$ to 46, we also observe large probability to stay in the initial state and large spread around final n. In figure 11, we consider microwave transitioning from $I = 40$ to 46 with 6-photon (left column) and $I = 40$ to 44 with 4-photon (right column) resonance conditions. Top panels in both columns show the probability binned in action. Three panels underneath these are the same phase space plots described above for figure 10. In the 6-photon case (left column), $F_K = 42$ V cm^{-1} at the peak (B1) and $F_K = 15$ V cm^{-1} on the rising (A1) and falling (C1) edges of the pulse. In the same manner, in the 4-photon case (right column), $F_K = 26$ V cm^{-1} at the peak (B2) and $F = 15$ V cm^{-1} at the rising (A2) and falling (C2) edges. Roughly 70% of the population transitions into $I = 44$ for the 4-photon resonance condition with virtually no spread in final n. This is in contrast with the 6-photon transition case as the top-left panel in figure 11 shows little population transferred into $n = 46$. Furthermore, we observe ∼52% trajectories ionize. This large probability of ionization is again due to the fact that at the peak of the microwave pulse, the entire region of phase space above the main island is dissolved into the chaotic sea. Trajectories that mix into the chaotic sea freely drift to higher I and eventually ionize. Still about half

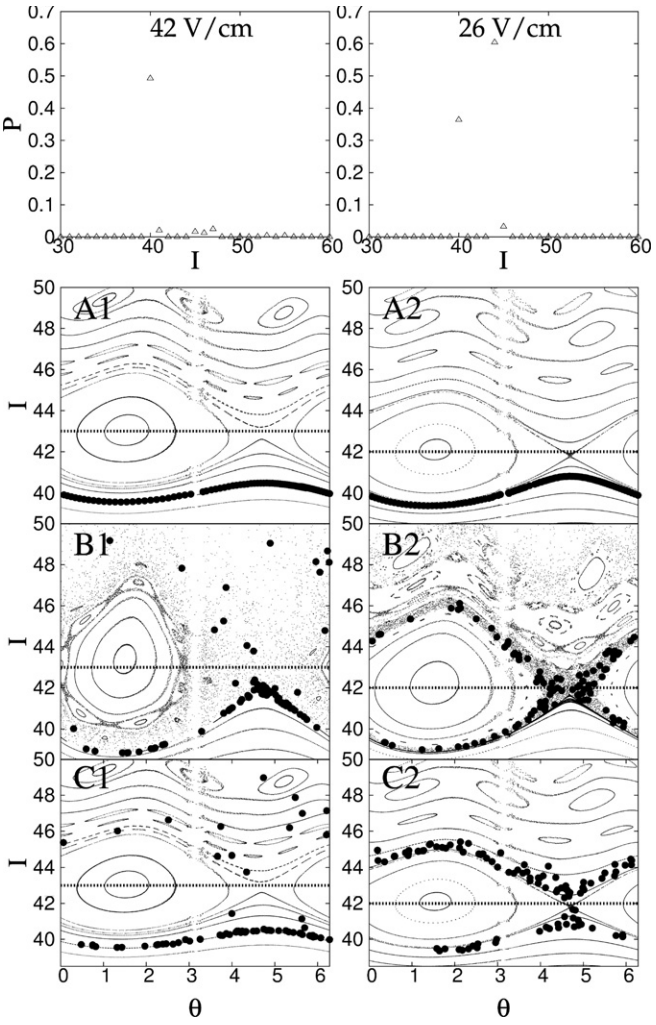

Figure 11. Similar to figure 10 but for the 6-photon and 4-photon resonance conditions for microwave driving of $n = 40$ discussed in the text. The top panels show probabilities binned in action. For the 6-photon resonance condition, the transitioning out of $I = 40$ only results in ionization, whereas for the 4-photon transition ∼64% of the population is transferred to $I = 44$. The larger driving field in the 6-photon case results in complete destruction of the regular structures above the island, whereas the 4-photon case retains these structures, constricting the chaotic sea into a narrow band.

of the population sticks to the initial $I = 40$ KAM surface as in the 8-photon transition depicted in figure 10(b). Higher rate of transition with no spread in final n in the 4-photon resonance condition results from the fact that at the peak of the microwave pulse, $F_K = 26$ V cm^{-1} and the chaotic sea straddling the main island does not extend above the final I that we target. This shows that the mechanism discussed in [15] still works, but in this case the atom can only make smaller Δn transitions. From the right column, it is evident that as the initial $I = 40$ surface is destroyed, the trajectories mix into the chaotic sea which only spans a region big enough for the trajectories to swing around the main island as in [15]. Comparison between figures 11(B1) and (B2) clearly shows that extent of the chaotic sea is increased when the system is driven harder resulting in the ionization of the wandering trajectories in the chaotic sea.

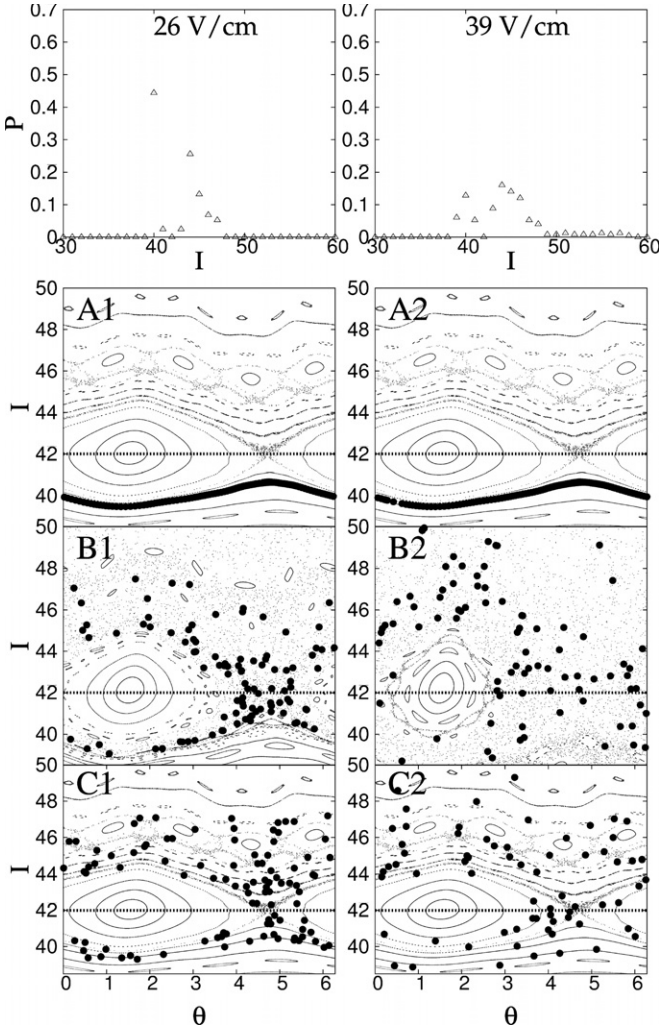

Figure 12. Same as figure 11 but for two different peak field strengths of $F_K = 26$ V cm^{-1} and $F_K = 39$ V cm^{-1} for $\sin^3(\omega t)$ 'kicked' atom using the 4-photon resonance condition. As in figure 11, driving the system harder destroys the stable structures above the main island creating a chaotic sea that extends high up in action.

For the kicked atom, we use bidirectional $\sin^3(\omega t)$ pulses as the trajectories start from $t = 0$. Figure 12 is for 4-photon transitioning from $I = 40$ to 44 with $F_K = 26$ V cm^{-1} (right column) and $F_K = 39$ V cm^{-1} (left column). The top panels again show probabilities binned in action, and underneath each are shown the phase space plots as in figure 11. For the weaker kicked case with $F_K = 26$ V cm^{-1}, roughly 25% of the population transitions into $I = 44$ with ~20% spread over adjacent I. About 45% of the populations stays in $I = 44$. In the corresponding phase space plots A1, B1 and C1, the peak field strengths are $F = 15$, 26 and 15 V cm^{-1} respectively. Note that although the chaotic sea extends high in action, there are still small bands of stable islands above $I = 46$ which act as a barrier preventing the trajectories to drift up freely. This results in a small band of final I around $I = 44$ and hinders ionization for the duration of the pulse envelope. When the atom is kicked harder using $F_K = 39$ V cm^{-1} in the right column, the stable structures above the main island are destroyed and now the chaotic sea extends high up in I (B2) without any barriers. This results in a high rate of ionization and a large spread of population above the main island of stability. From the top-right panel in figure 12, roughly 55% of the population is spread over in $I = 43$ and higher, whereas ~25% show a small spread near the initial I. The remaining ~35% ionizes by drifting up in I once mixed into the chaotic sea (B2 and C2). This also points out to the importance of the duration of the pulse at its peak strength. Longer the pulse remains on, higher up in I the trajectories can drift giving larger spread in final I. On the other hand, if the pulse is turned off, short after the trajectories are mixed into the chaotic sea, they can be trapped in a much narrower band near the intended final I.

Comparing the 4-photon microwave case in figure 11 with the 4-photon transitioning in the kicked atom in figure 12, we note that when the microwave was driven, larger fraction of the population transitions into $I = 44$ with virtually no spread over final I. The probability for transitioning out of $I = 40$ is relatively decreased when the atom is kicked and the final population has a spread over I near $I = 44$. The reason behind this discrepancy can be seen when the surfaces of the sections shown in figures 11(B1) and 12(B1) are compared for both of which $F_K = 26$ V cm^{-1}. In the microwave-driven case, the chaotic sea is only large enough for the trajectories to swing around the main island, whereas in the kicked atom, its extent is much larger giving rise to diffusion of the trajectories in a much larger region of the phase space.

5. Conclusions

Using a flat-top pulse of bidirectional kicks, we compared microwave driving to cases where microwave HCPs are replaced by narrower HCPs whose extreme limit gives impulsive kicks. We have found that achieving efficient population transfer gets harder as the microwave HCPs start to become narrower kicks as we demonstrated by driving the 8-photon resonance condition to excite the $n = 72$, $\ell = 1$ state up to the $n = 80$ manifold. We also observed very poor transfer efficiency when we kicked atoms in the $n = 40$, $\ell = 1$ state up to the $n = 46$ manifold through the 6-photon resonance condition using unidirectional kicks. In the long time limit, most of the population transferred into the $n = 46$ manifold is excited further up to $n = 52$ by chirping through an accidental 4-photon resonance that connects $n = 46$ with $n = 52$. Besides initially preparing the atom in a field-free atomic eigenstate, we also tried to start from Stark states. This did not particularly improve the transfer efficiency over the cases when the atom was initially in a field-free eigenstate. We tried starting from both the red-most and the central Stark states. Both initial states resulted in ℓ distributions in the final n-manifold largely imitating that in the corresponding initial Stark state.

By turning off the flat-top envelope as soon as it peaks, we were able to achieve efficient population transfer through a 6-photon resonance condition by subjecting 40p Li atoms to unidirectional electric field impulses of durations much less than the classical orbital period of the Rydberg electron. Using

unidirectional kicks, we were able to transfer ∼76% of the population into the $n = 46$ manifold with angular momenta confined to $\ell < 5$. Such multiphoton transitions have been shown to yield a final population with large ℓ spread when microwaves are used [15].

Our three-dimensional CTMC simulations for the population transfer through an 8-photon resonance condition yielded similar efficiencies as our quantum calculations. We progressively reduced the width of the microwave HCPs into bidirectional $\cos^3(\omega t)$ kicks. To investigate this suppression of transfer efficiency, we used a one-dimensional classical model where we 'kicked' hydrogen atoms by bidirectional $\sin^3(\omega t)$ kicks to peek into the mechanisms taking place inside the classical phase space. As in the microwave-driven case, the trajectories starting on a stable surface just below the main island of stability need to mix into the chaotic sea to swing around the island to reach the final state. For the final state distribution to be sharp, the extent of the chaotic sea should go just above the main island. We did not see this happen in the kicked atom, with chaotic sea reaching high up in effective n. On the other hand, small islands of stability are formed above the main island and near the initial stable surface which prevents trajectories from freely drifting high up in n. This results in a wider spread of final states after the kicks are turned off when compared with the microwave-driven case. Kicking the atom even harder results in the destruction of these stable structures above the main island which leads to both very large spreads of final state distributions and ionization. The same problem also occurs for weaker kicked but higher order multiphoton transitions.

Acknowledgments

This work was supported by the Office of Basic Energy Sciences and the Office of Fusion Energy Sciences, US Department of Energy.

References

[1] Frey M T, Dunning F B, Reinhold C O, Yoshida S and Burgdörfer J 1999 *Phys. Rev.* A **59** 1434
[2] Reinhold C O, Yoshida S, Burgdörfer J, Zhao W, Mestayer J J, Lancaster J C and Dunning F B 2006 *Phys. Rev.* A **73** 033420
[3] Persson E, Fürthauer S, Wimberger S and Burgdörfer J 2006 *Phys. Rev.* A **74** 053417
[4] Tannian B E, Stokely C L, Dunning F B, Reinhold C O, Yoshida S and Burgdörfer J 2000 *Phys. Rev.* A **62** 043402
[5] Zhao W, Mestayer J J, Lancaster J C, Dunning F B, Reinhold C O, Yoshida S and Burgdörfer J 2006 *Phys. Rev.* A **73** 015401
[6] Yoshida S, Reinhold C O, Kristöfel P and Burgdörfer J 2000 *Phys. Rev.* A **62** 023408
[7] Klews M and Schweizer W 2001 *Phys. Rev.* A **64** 053403
[8] Gleyzes S, Kuhr S, Guerlin C, Bernu J, Deleglise S, Hoff U B, Brune M, Raimond1 J-M and Haroche S 2007 *Nature (London)* **446** 297
[9] Gross M and Liang J 1986 *Phys. Rev. Lett.* **57** 3160
[10] Dunning F B, Mestayer J J, Reinhold C O, Yoshida S and Burgdörfer J 2009 *J. Phys. B: At. Mol. Opt. Phys.* **42** 022001
[11] Yoshida S, Reinhold C O, Burgdörfer J, Mestayer J J, Lancaster J C and Dunning F B 2008 *Phys. Rev.* A **77** 013411
[12] Yoshida S, Reinhold C O, Persson E, Burgdörfer J and Dunning F B 2005 *J. Phys. B: At. Mol. Opt. Phys.* **38** S209
[13] Mestayer J J, Wyker B, Lancaster J C, Dunning F B, Reinhold C O, Yoshida S and Burgdörfer J 2008 *Phys. Rev. Lett.* **100** 243004
[14] Maeda H, Norum D V L and Gallagher T F 2006 *Phys. Rev. Lett.* **96** 073002
[15] Topçu T and Robicheaux F 2009 *J. Phys. B: At. Mol. Opt. Phys.* **42** 044014
[16] Topçu T and Robicheaux F 2007 *J. Phys. B: At. Mol. Opt. Phys.* **40** 1925
[17] Wesdorp C, Robicheaux F and Noordam L D 2001 *Phys. Rev. Lett.* **87** 083001
[18] Mitchell K A, Handley J P, Tighe B, Flower A and Delos J B 2004 *Phys. Rev. Lett.* **92** 073001
[19] Stevens M J and Sundaram B 1987 *Phys. Rev.* A **36** 417